

Steady state stability assessment of voltage source converter in a DC microgrid under weak grid conditions

Ganeshan Viswanathan¹, Govindanayakanapalya Venkatagiriappa Jayaramaiah²

¹Department of Electronics and Communication Engineering, Dr. Ambedkar Institute of Technology, Bangalore,
(Affiliated to Visvesvaraya Technological University, Belgaum), India

²Department of Electrical and Electronics Engineering, Dr. Ambedkar Institute of Technology, Bangalore,
(Affiliated to Visvesvaraya Technological University, Belgaum), India

Article Info

Article history:

Received May 21, 2023

Revised Oct 27, 2023

Accepted Nov 16, 2023

Keywords:

Droop controller

Islanded microgrid

Steady-state stability
assessment

Support vector machine

Voltage source inverters

ABSTRACT

Traditionally, steady-state assessment involves analyzing numerous variables using Eigen analysis. This paper presents a decision support application for diagnosing the steady-state assessment of droop-controlled voltage source inverters in islanded microgrid operations or weak grid operations with reduced input attributes. This paper proposes an approach using feature extraction from the state space variables of the droop-controlled voltage source inverter (VSI). Photovoltaic (PV) and wind energy sources are considered with their stipulated power-delivering capability considered. To improve the generalization of the predictive model, preprocessing techniques are employed to eliminate data distortions. Dimensionality reduction is achieved through principal component analysis (PCA) applied to the steady-state variables. The evaluation of the VSI's steady-state stability is conducted utilizing support vector classification algorithm. To ascertain the reliability of the steady-state stability classification, an assessment of the support vector machine (SVM) model's performance is carried out, which includes the examination of metrics like the area under the curve (AUC) and the receiver operating characteristics (ROC) curve. The findings from the assessment of VSI's steady-state stability indicate a commendable level of performance, achieving an accuracy rate of 93.5%.

This is an open access article under the [CC BY-SA](https://creativecommons.org/licenses/by-sa/4.0/) license.



Corresponding Author:

Ganeshan Viswanathan

Department of Electronics and Communication Engineering, Dr. Ambedkar Institute of Technology

(Affiliated to Visvesvaraya Technological University, Belgaum)

Bangalore, India

Email: ganeshanvisu@gmail.com

1. INTRODUCTION

Distributed generators can be installed in rural areas using the right power electronics converters. The islanded mode of the distributed generators (DG's) operation helps with rural electrification because of its autonomous operation. The connection between the primary grid and the DGs operates in a stiff grid mode, wherein voltage and frequency measurements derived from the primary grid assume the phase-locked loop (PLL)-based synchronization, a concept in the study by Dağ and Aydemir [1]. Analyzing the stability of an islanded microgrid is a complex process that requires the examination of steady-state variables and performing eigen analysis on those variables [1]. The stability assessment of an islanded microgrid involves studying the behavior of steady-state variables and performing eigen analysis to determine its stability.

Microgrids working in islanded mode adopt the droop controller for voltage and frequency regulation as discussed by Rajamand [2]. Inverters connected in parallel are synchronized using the droop controller. They

also act as an effective power-sharing strategy. Instability due to changing load from each inverter is regulated by the droop controller. In islanded mode, these VSI need to self-synchronize and distribute power to the load. This setup of the voltage source inverters (VSIs) called parallel inverters is supplied from renewable energy resources as discussed by Sanabria *et al.* [3], and Veerashekar *et al.* [4]. The stability study of an autonomous microgrid, which incorporates a combination of a renewable energy source and a diesel generator, focuses on investigating the droop control method. During fault situations, deliberate intentional power reduction from the renewable source results in a loss of synchronization in the diesel generator. In an islanded microgrid setup, the power-sharing capability of inverters can be disturbed by harmonic resonance, which occurs when multiple inverters are connected in parallel. Harmonic resonance is an instability that affects the system and hinders the efficient sharing of power among the inverters. The number of parallel inverters that can be connected in the grid-connected microgrid environment is decided by impedance-based calculations [5] with stability as the constraint. A nonlinear model of the network sensed the resonance mode from the network as discussed by Cabero and Prodanovic [6]. Offshore inverters with long cables are introduced to impedance-based stability analysis. Three different inverters and non-negligible lengthy cables are used for the stability investigation. Inverter's fault ride-through capability is exploited using the droop controller in the multiple resonant converters and the state space model is developed to explore the stability limit of the parallel inverters [7].

A magnitude reshaping strategy is implemented to improve the stability of the parallel inverters in the weak grid environment when the Nyquist stability criterion is complicated since the impedance ratio of the grid-connected system is insufficient to satisfy the criterion [8]. A region-based stability analysis is developed on active dampers of the AC microgrid environment [9]. This method provides a parameter selection of the active damper, making it more flexible. The output impedance of the voltage source converter (VSC) is controlled by finding the difference between the real and reactive power observed from both the inverter output and the point of common coupling (PCC) [10]. The virtual impedance is controlled by varying X/R ratio at the inverter output thus acting as the damping controller at the PCC. Low-frequency oscillations in isolated microgrid with battery energy storage and fueled by renewable energy source is investigated with smart loads [11]. Oscillations are associated with the droop controller of the interfaced distributed generators (DGs). Stability analysis using the linearized state space model is developed by extending it to the smart loads, which depicts the impact of low-frequency oscillations on the islanded microgrid. A microgrid with four RES working both in grid-connected and islanded mode is controlled using the three hierarchical controllers which can handle both the small signal and large signal disturbances [12]. The nonlinear fuzzy logic controller which controls the reactive power increases the ride-through capability and system stability margins. An improved virtual impedance method called the distributed adaptive virtual impedance control (DAVIC) is used to coordinate the virtual impedance of the inverter automatically using global information. The difference between the active power of a local module and the average active power of all the other modules of the uninterrupted power supply (UPS) is measured to obtain the virtual impedance thus providing an enhanced power-sharing capability of the parallel inverters [13]. A small AC signal (SACS) is injected into the output of the inverter to control the unbalanced and harmonic power by the use of the adaptive virtual impedance control method [14]. Injected SACS synchronizes the inverters and adjusts the selected harmonic frequencies and fundamental negative sequences. A low X/R ratio in the power lines impedance and no inertia in the inverter-based microgrids demand a better droop controller in the microgrid with multiple renewable energy sources. A novel consensus protocol using fuzzy logic is developed that takes care of both the power-sharing capability of the droop controller and power quality enhancement using average voltage profile restoration [15]. Stability analysis in AC/DC hybrid microgrid for a varied range of R and X for the microgrid cables. Frequency is controlled by controlling the reactive power with resistive cables and active power with inductive cables [16]. The flexibility of renewable energy-based islanded microgrids is enhanced using electric springs. Electric springs is the device that can improve the power quality issues in the islanded microgrid by effectively regulating the supply voltage. A model predictive controller is applied on the non-critical loads like the water heating system on the electric springs to effectively control the voltage regulation [17] and sensitivity analysis on the ramping capability of a microgrid is observed.

The small-time constants of the power electronic devices make the small signal stability a challenge in the power electronics-based power system. The power system is thus divided into smaller portions and individual components like inverter, load, and impedances and state space models of these portions are algebraically assembled to validate the stability analysis [18]. The distribution network's linearized state space model connected with electric springs is developed which can later add the inverter interfacing with DG, batteries, and loads. Analysis including the effect of the R/X ratio, the impact of distance between the distribution network and the electric spring, and the effect of proximity between different electric springs on the stability is discussed [19]. Although traditional droop controllers are capable of power-sharing between the parallel inverters, the mismatch in impedances of the parallel inverters introduces reactive power that is unequal between the inverters. Reactive power-sharing in parallel inverters is developed using the novel droop controller called the adaptive virtual impedance controller. Optimal control parameters are obtained using the

small signal stability analysis of the parallel inverters using the adaptive controller [20]. A photovoltaic (PV) inverter with a non-renewable energy-based generator when connected in the islanded mode without energy storage need to regulate the maximum power generated from the PV inverter. Power wastage due to power more than the load demand and unstable power due to power less than the load demand at the PV inverter is experienced. An improved droop control loop is utilized to increase the utilization efficiency of the PV power and also maintain the system stability [21]. A current sharing strategy between the grid and the parallel inverter system in a grid-connected microgrid with master-slave topology is developed using the self-constructing fuzzy neural network (SFNN). The SFNN imitates the sliding mode controller that implements grid-connected current tracking in the grid-connected microgrid topology [22].

Multi-inverter grid connected system experiences instability due to resonance caused by grid impedances. A multi-input, multi-output matrix is generated which involves both the self-stability of the multi-inverter and interactive stability since it is grid connected. The grid impedance effect on the multi-inverter is nullified by adopting the phase-lead compensator which improves the robustness of multi-inverter control when connected to the grid [23]. The feeder impedance estimation method is developed in a non-invasive method. It is first deducted that the inverter impedance is negligible in the lower-order harmonics and then the feeder impedance is calculated using the current and voltage at a specific harmonic frequency. This feeder impedance is introduced as the virtual impedance and power-sharing capability is enhanced using a hierarchical control structure [24]. Instead of the conventional stability assessment using the characteristic equations from the state space model, system synchronization stability is localized to inverters. The passive synchronization behavior of the inverters is considered to analyze the stability [25]. Impedance-based stability analysis is adopted in such a system by modeling the equivalent circuit of the transmission line as a current source grid. Both Euler's formula and Nyquist's stability criterion are used to assess the stability of the system [26]. The dynamics in the current controller of the phase locked loop (PLL) controlled grid-connected parallel inverters deteriorate when connected to a weak grid. This negative effect of the PLL is compensated using the proportional integral (PI) controller combined with the capacitive-current-feedback active damping strategy [27]. A complete stability analysis of the parallel inverters in weak grid condition is discussed in [28]. Eigen analysis is used to find the stability of the system with virtual impedance method. Various contributions from researchers on Microgrid and intelligent controllers on microgrid can be witnessed in literatures [29]–[36].

Previous literature has discussed the stability assessment in islanded microgrids using different analytical methods. This paper attempts to assess the steady-state stability in the islanded microgrid using machine learning methods with feature extraction-based data preprocessing techniques on the state space attributes. Support vector machine is used as the machine learning algorithm to predict the steady-state assessment for the islanded microgrid using PCA. The average modeling of the droop-controlled islanded microgrid is discussed in section 2, the steady-state prediction algorithm is discussed in section 3 and the results and discussion of the proposed implementation are discussed in section 4 followed by the conclusion and references.

2. STATE SPACE MODEL OF DROOP-CONTROLLED ISLANDED MICROGRID

The steady-state stability of the synchronous machines defines the condition that allows two machines to work in synchronism. Similarly, islanded microgrids controlled using droop control in an islanded mode need to be analyzed for steady-state stability. The droop controller of the islanded microgrid is based on the synchronous generator's power balancing principles. The comprehensive droop control system for the islanded microgrid is illustrated in the block diagram provided in Figure 1. Within this diagram, the inverter's droop controller, equipped with the inductance capacitance inductance (LCL) filter, is depicted. The microgrid employs two inverters operating in parallel, with one serving as the master inverter and the other as the slave inverter. This arrangement ensures that one inverter acts as the reference for maintaining voltage and frequency consistency in the other inverter. The voltage source inverter (VSI) mentioned in Figure 1 is one of the islanded microgrids which will act as either the master or the slave inverter. Similarly, another inverter with the droop controller is used for the droop controller that synchronizes with the VSI shown in Figure 1. The droop controller starts with the calculation of instantaneous real power and reactive power from the inverter output. The current measured after the inductance and capacitance of the LCL filter at the inverter output is used to obtain the direct axis voltage and current, and quadrature axis voltage and current denoted as v_{odr} , i_{odr} , v_{oqr} , and i_{oqr} . Instantaneous real and reactive power is calculated using these four attributes and a low pass filter is applied to get the stable real and reactive power as given in (1) and (2). The inverter is modeled using these real and reactive power equations.

$$P_{\text{filt}} = \omega_{\text{corn}} p_{\text{inst}} / (s + \omega_{\text{corn}}) = -p_{\text{inst}} \omega_{\text{corn}} + 1.5 \omega_c (v_{odr} i_{odr} + v_{oqr} i_{oqr}) \quad (1)$$

$$Q_{\text{filt}} = \omega_{\text{corn}} q_{\text{inst}} / (s + \omega_{\text{corn}}) = -q_{\text{inst}} \omega_{\text{corn}} + 1.5 \omega_c (v_{oqr} i_{odr} - v_{odr} i_{oqr}) \tag{2}$$

Here p_{inst} and q_{inst} are instantaneous real and reactive power and P_{filt} and Q_{filt} are smoothed real and reactive power respectively and ω_c is the corner frequency. When connected to the weak grid, the inverter generates the reference voltage and angular frequency using droop characteristics, acting like a synchronous machine to determine the voltage and phase angle from the droop curves, we leverage the smoothed real and reactive power curves. These droop curves illustrate the relationship between real power and angular frequency ($P-\omega$) as well as reactive power and voltage ($Q-V$). Analyzing these curves allows for the derivation of voltage and phase angle information. The use of the smoothed power curve enhances the accuracy and reliability of this information, facilitating efficient system monitoring and control. The slopes, denoted as ' m_{ω} ' and ' m_{volts} ' are extracted from the droop curves by examining angular frequency for real power variations and voltage for reactive power variations, as depicted in Figures 2(a) and 2(b), respectively. The droop characteristics graph from Figure 1 generates instantaneous voltage and angular frequency based on the calculated real and reactive power.

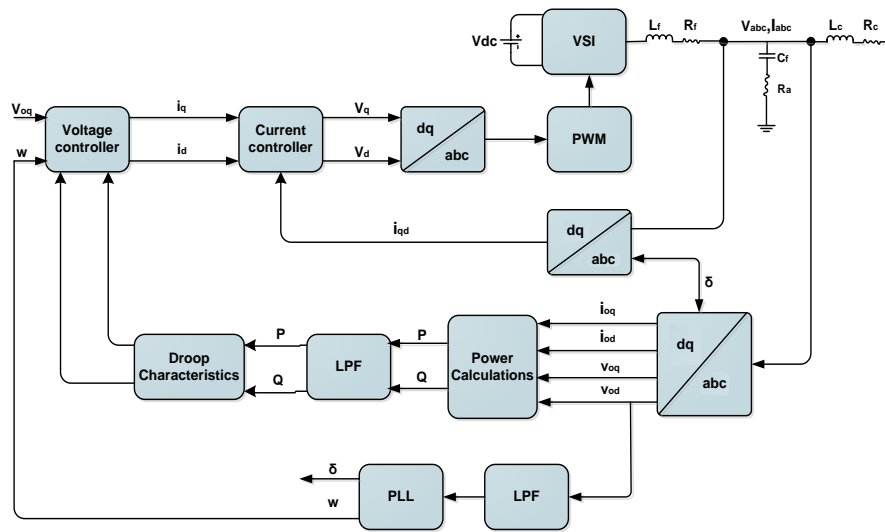


Figure 1. Droop controller of inverter with LCL filter

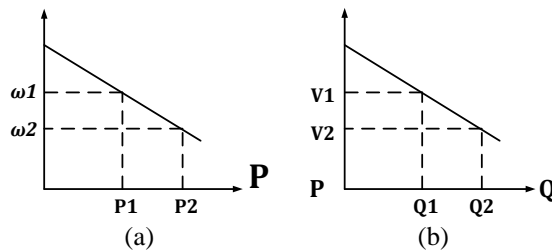


Figure 2. Droop curves (a) real power (P) versus Angular frequency(ω) and (b) reactive power (Q) versus voltage (V)

The voltage source inverter (VSI) shown in Figure 1 is supplied with the DC power supply. When PV and Wind are connected it is variable. This paper uses the controlled three-phase supply with active and reactive power limits to represent PV and Wind sources. The slope from the droop characteristic curve m_{ω} and m_{volts} is calculated using the formula as given in (3) and (4). As shown in (5) and (6) provide a means to compute the reference angular frequency and reference voltage by assessing the disparity between the system's current instantaneous power outputs (P_{filt} and Q_{filt}) and the desired power outputs (P_{filtref} and Q_{filtref}). Control systems rely on these reference values to adjust the operation of generators and other power equipment, ensuring the maintenance of the required frequency and voltage levels. These reference values are derived from the instantaneous real power and reactive power, enabling the calculation of instantaneous angular frequency and voltage.

$$m_{\omega} = (\omega_1 - \omega_2) / (P_{2\text{filt}} - P_{1\text{filt}}) \quad (3)$$

$$m_{\text{volts}} = (v_1 - v_2) / (Q_{2\text{filt}} - Q_{1\text{filt}}) \quad (4)$$

$$\omega_{\text{ref}}^* = \omega_{\text{nat}} - m_{\omega} P_{\text{filt}} \quad (5)$$

$$v_{oq}^*_{\text{ref}} = v_{oq} - m_{\text{volts}} Q_{\text{filt}} \quad (6)$$

Here ω_1, ω_2 are different angular frequency instants chosen from the droop curve in Figure 2. Whenever the inverter produces sinusoidal output at 60 Hz, $P_{1\text{filt}}$, and $P_{2\text{filt}}$ represent actual power amplitude samples. The reference quadrature axis voltage component ($v_{oq}^*_{\text{ref}}$), and the reference angular frequency (ω_{ref}^*) are critical for synchronization and can be found using (5) and (6). The phase-locked loop (PLL) controller, which depends on a proportional-integral (PI) controller to produce inputs for voltage and current regulation, cannot function without these computations. Before comparison, the input undergoes filtering through a low-pass filter with a corner frequency of $\omega_{c,\text{pll}}$ to ensure consistent synchronization frequency. The phase-locked loop locks the instantaneous angle to a reference value of 377 (in rad/sec for a 60 Hz frequency), while the direct axis voltage is regulated to zero within the PLL. The PLL, responsible for generating the angle δ , is depicted in Figure 3.

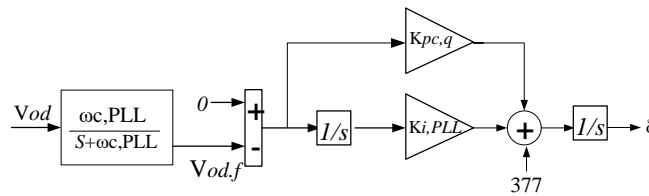


Figure 3. The instantaneous angle from PLL

The controller is used to derive the PI controllers that produce the reference currents in the direct axis and quadrature axis. These PI controllers are essential to the voltage controller's functionality. They contribute to the state equations of the voltage controller, as shown by (7) and (8), by providing the necessary reference current values. The direct and quadrature axes' currents are properly regulated by the PI controllers, allowing for precise control and stabilization of the system.

The direct axis reference current ($i_{d}^*_{\text{ref}}$) and quadrature axis reference current ($i_{q}^*_{\text{ref}}$) as they flow through the filter capacitor (LCL) are crucially determined by (7) and (8). These equations involve both proportional and integral gains, which are expressed as ($k_{\text{ivgain},d}$, $k_{\text{pvgain},d}$) for quadrature axis reference current generation and ($k_{\text{ivgain},q}$, $k_{\text{pvgain},q}$) for direct axis reference current generation. Utilizing these gains allows the system to accurately compute and regulate the reference currents in both the direct and quadrature axes, contributing to overall control and system stability.

$$\Phi_{d'}_{\text{ref}} = \omega_{\text{PLL}} - \omega_{\text{ref}}^* ; i_{d}^*_{\text{ref}} = k_{\text{ivgain},d} \Phi_{d'} + k_{\text{pvgain},d} \Phi_{d'}_{\text{ref}} \quad (7)$$

$$\Phi_{q'}_{\text{ref}} = v_{oq}^*_{\text{ref}} - v_o ; i_{q}^*_{\text{ref}} = k_{\text{ivgain},q} \Phi_{q'} + k_{\text{pvgain},q} \Phi_{q'}_{\text{ref}} \quad (8)$$

The angular frequency variation relative to the reference, represented as $\Phi_{d'}_{\text{ref}}$, and the voltage change relative to the reference, denoted as $\Phi_{q'}_{\text{ref}}$, are derived from the droop characteristics. These values signify the deviations from the intended reference values. The voltage controller receives its input from the current reference. The output currents from the LCL filter are measured, and a comparator assesses them against the reference current. Both the reference voltage $v_{id}^*_{\text{ref}}$ and the reference voltage $v_{iq}^*_{\text{ref}}$ are generated by the current controller. This comparison is orchestrated by the current controller, which regulates the inverter using space vector pulse width modulation (SVPWM), as depicted in Figures 4(a) and 4(b). The state equations for generating the quadrature axis voltage reference v_{iq} and the direct axis voltage reference v_{id} are given in (9) and (10).

$$v_{id}^*_{\text{ref}} = -\omega_{\text{inst}} L_f i_{iq} + k_{ic} \sum (i_{d}^*_{\text{ref}} - i_{d}) + k_{pc,d} \sum (i_{d}^*_{\text{ref}} - i_{d}) \quad (9)$$

$$v_{iq}^*_{\text{ref}} = -\omega_{\text{nat}} L_f i_{id} + k_{ic} \sum (i_{q}^*_{\text{ref}} - i_{q}) + k_{pc,q} \sum (i_{q}^*_{\text{ref}} - i_{q}) \quad (10)$$

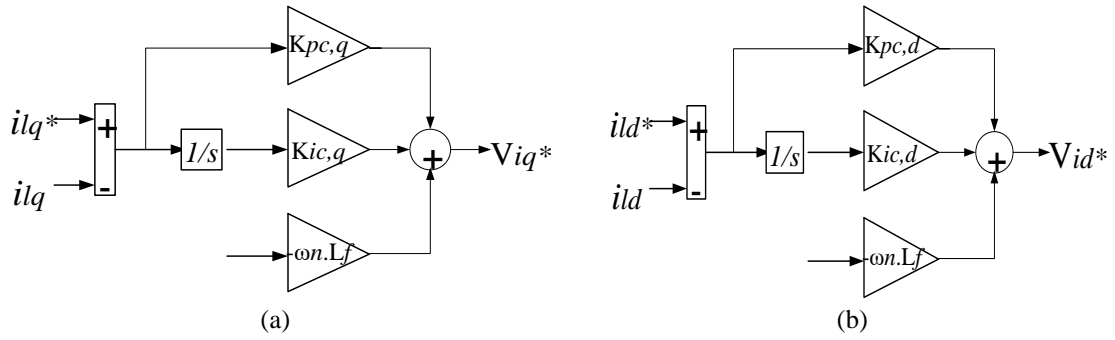


Figure 4. Voltage reference generators (a) quadrature axis voltage and (b) direct axis voltage

The PI controller employs the proportional gain (k_{pcd} for direct axis and k_{pcq} for quadrature axis) and integral gain (k_{icd} for direct axis and k_{icq} for quadrature axis) to determine the direct and quadrature axis voltage references. The discrepancy between the actual (without the asterisk *) and reference direct (i_{ld} , i_{ldref}^*) and quadrature (i_{lq} , i_{lqref}^*) currents serves as the input to the PI controller. The current controller generates a control voltage, which functions as the reference voltages. The LCL filter includes a damping resistor (R_d), the filter capacitor (C_f), and parasitic resistances like r_f for the filter inductor (L_f) and r_c for the capacitor (L_c). The state equations controlling the LCL filter's filter properties are defined by (11) through (12).

$$\dot{i}_{ld}'' = 1/L_f (-r_f i_{ld} + v_{id} + v_{od}) + \omega_{PLL} i_{lq} \quad (11)$$

$$\dot{i}_{lq}'' = 1/L_f (-r_f i_{lq} + v_{iq} + v_{oq}) + \omega_{PLL} i_{ld} \quad (12)$$

According to (11) and (12) provide a detailed representation of the direct axis current (i_{ld}'') and the quadrature axis current (i_{lq}'') within the LCL filter. These currents are explicitly described by equations (13) and (14), indicating the current flow from the capacitor to the load-side inductor within the LCL filter. The (15) and (16) define the load-side direct axis voltage (v_{od}') and quadrature axis voltage (v_{oq}') within the LCL filter, establishing the voltage characteristics associated with the direct and quadrature axes of the load-side components in the LCL filter.

$$i_{od}'' = 1/L_c (-r_c i_{oq} + v_{od} - v_{bd}) - \omega_{PLL} i_{oq} \quad (13)$$

$$i_{oq}'' = 1/L_c (-r_c i_{od} + v_{oq} - v_{bq}) - \omega_{PLL} i_{od} \quad (14)$$

$$v_{od}' = 1/C_f (i_{ld} - i_{od}) + \omega_{PLL} v_{oq} + R_d (i_{ld} - i_{od}) \quad (15)$$

$$v_{oq}' = 1/C_f (i_{lq} - i_{oq}) + \omega_{PLL} v_{od} + (i_{lq} - i_{oq}) \quad (16)$$

In order to introduce load dynamics into the system, perturbation elements are used in the assessment of islanded microgrid stability. As shown in (17) and (18) are the state equations that describe the dynamic behavior. The load quadrature axis current ($i_{load,Q}$) is defined by (18), whereas the load direct axis current ($i_{load,D}$) is defined by (17). These equations, which take into account the direct and quadrature axes, describe the behavior and flow of current in the load. It is possible to gain a deeper knowledge of the stability and performance of the islanded microgrid by taking into account these load dynamics. The state equations contribute to a thorough understanding of the stability of the system by offering insightful information about how the load currents change over time.

$$\dot{i}_{loadD} = 1/L_{load} (-R_{load} i_{loadD} + V_{bd}) + \omega_{pll} i_{loadQ} \quad (17)$$

$$\dot{i}_{loadQ} = 1/L_{load} (-R_{load} i_{loadQ} + V_{bq}) - \omega_{pll} i_{loadD} \quad (18)$$

The total resistance and inductance of the load are shown by the distribution line. These lines play crucial roles in determining how the inverter responds to load disturbances since they are coupled with other inverters in the distributed grid. As shown in (19) and (20), they provide the state equation for the distribution line. Both the subscript "i" and the subscript "j" belong to distributed energy resources (DER1) (PV) & DER2 (Wind). Distribution line connecting these two DERs. Amongst "i" and "j" DERs, there exists a direct axis current ($i_{lineD_{ij}}$) and a quadrature axis current ($i_{lineQ_{ij}}$).

$$\dot{i}_{lineDij} = 1/L_{line} (r_{line}\dot{i}_{lineD} + v_{bDj} - v_{bDi}) + \omega_{pll}\dot{i}_{lineQ} \quad (19)$$

$$\dot{i}_{lineQij} = 1/L_{line} (r_{line}\dot{i}_{lineQ} + v_{bQj} - v_{bQi}) + \omega_{pll}\dot{i}_{lineD} \quad (20)$$

The direct and quadrature voltages at the "ith" DER are shown by the variables $v_{bD,i}$, $v_{bQ,i}$, r_{line} , and L_{line} , which stand for the line resistance and line inductance between the two DERs, respectively. Direct and quadrature voltages are present at the "jth" DER, respectively. The average model is utilized to calculate the state variables of this islanded microgrid. These state variables are linearized in order to perform an Eigen analysis for stability analysis.

3. RESULTS AND DISCUSSION

Table 1 displays the input parameters for the simulation. The development of the average model for the islanded microgrid is carried out using MATLAB/Simulink, with the variables detailed in Table 1. In accordance with Figure 1 and as explained in the subsequent section, MATLAB simulation is employed to conduct an analysis of stability and feature reduction, with two inverters connected in parallel.

Table 1. Parameters of droop controlled islanded microgrid [28]

Parameter	Value	Parameter	Value
ω_{pll}	377 rad/s	n	1/1000 V/var
ω_n	377 rad/s	m	1/1000 rad/Ws
$V_{oq,n}$	85 V	$\omega_{c,pll}$	7853.98 rad/s
L_{line}	0.40 mH	ω_c	50.26 rad/s
r_{line}	0.15 Ω	C_f	15 μ F
R_{pert}	25 Ω	R_d	2.2025
L_{pert}	7.50 mH	L_c	0.50 mH
L_{load}	15 mH	r_f	0.50 Ω
R_{load}	25 Ω	L_f	4.20 mH
r_n	1000	r_c	0.09 Ω

3.1. State space variables of droop-controlled islanded microgrids

X_{inv1} , X_{inv2} , and X_{load} are the state variables for each of the three variables: DER1, DER2, and load. The process of gathering the equilibrium values, steady-state values, or state variables that are shown in (21)-(24) is referred to as the linearization of these parameters. One master vector is created by combining the vectors, as illustrated in (25)

$$x_{inv1} = (\delta1P1Q1\Phi d1\Phi q1\gamma d1\gamma q1ild1ilq1vod1voq1iod1ioq1\Phi PLL1vod1,) \quad (21)$$

$$x_{inv2} = (\delta2P2Q2\Phi d2\Phi q2\gamma d2\gamma q2ild2ilq2vod2voq2iod2ioq2\Phi PLL2vod2,) \quad (22)$$

$$x_{load} = [iloadD1iloadQ1iloadD2iloadQ2] \quad (23)$$

$$x_{line} = [ilineD21ilineQ21] \quad (24)$$

$$x = [x_{inv1} \ x_{inv2} \ x_{load} \ x_{line}] \quad (25)$$

In the typical model developed for linearization, an operational point of the variables defined in (25) is seen. For Eigen analysis, these consequently generated linearized values are used. The master vector specified in (25) is used to generate the state space (26). Here u stands for the inputs and x is the state vector. The following is the input vector defined in 27.

$$\dot{x} = Ax + Bu \quad (26)$$

$$u = [vbD1 \ vbQ1 \ vbD2 \ vbQ2] \quad (27)$$

To establish the total number of primary factors to be tested for islanded microgrid stability, the variables are processed for PCA analysis. PCA acts as the dimensionality reduction algorithm for the SVM-based steady-state prediction algorithm. The set of 36 variables indicated in (25) are obtained by measuring both the steady-state and unstable-state conditions during the operation of the islanded microgrid. These variables are then utilized as input for the principal component analysis (PCA) feature extraction algorithm. The measurement of these variables encompasses capturing data from various aspects of the microgrid, representing different

parameters and characteristics of the system. By incorporating measurements from both steady-state and unstable-state scenarios, a comprehensive dataset is obtained, encompassing a range of operating conditions.

3.2. PCA analysis

This dataset is used by the PCA feature extraction technique to find the most important variations and patterns within the measured variables. It seeks to capture the underlying structure of the system's behavior and decrease the complexity of the data while preserving crucial information. A more condensed representation of the dataset is generated by identifying pertinent features through PCA, enabling further analysis and decision-making procedures. The chosen features can then be applied to a variety of tasks, such as stability evaluation, fault detection, or control design, to improve knowledge of and control over the islanded microgrid. The system is unstable if the eigenvalues of the state space variables are positive in a steady state. Traditional steady-state estimation is replaced with machine learning-based steady-state assessment in the islanded microgrid. Instead of using the DC supply in the input of the inverter the three-phase source with a stipulated power limit is considered in order to obtain the out-of-synchronism condition for higher load conditions. Steady-state stability is disturbed when the power limit of the load is crossing the power limit of the renewable source. Load perturbation is applied in the droop-controlled islanded microgrid setup to analyze the stability of the system for load variations. R_{pert} and L_{pert} are the perturbation resistance and inductance values that are introduced at 3 seconds along with the load in the simulation running for 4 seconds. The MATLAB-based simulation developed using the specifications in Table 1 is supplied with the three-phase supply with the PQ bus configuration. Case 1 is run by stipulating the real power to 250 W and reactive power to 200 W from the PQ bus which is emulated to be a renewable energy source with limited power capability. The results obtained by applying the load within the steady state condition are given in Figures 5-7.

Figure 5 depicts that the load variation at 3 seconds in the simulation affects a small transient and again the angular rad/sec settles to 377 which corresponds to 60 Hz. Output analysis is conducted at the LCL filter's location, specifically after the LC segment of the filter, to assess the stability of both the inverter output and the droop controller. At this point, measurements of the direct and quadrature axis voltages and currents are obtained for both DER1 and DER2, which are operating in parallel.

The direct axis and quadrature axis current and voltage at the LCL filter during the steady state operation of the system is as shown in Figure 6. It can be observed that after the load variation applied at 3 secs the steady state condition continues with a minor transient in the voltage and current waveform. This steady state condition waveforms are used as the input data for the stability condition of the assessment carried out using SVM model.

A noteworthy observation is that there is a consistent correspondence between the voltage amplitude and the current amplitude. Thus, the synchronization is intact in this case. Even after the load variation at 3 Secs, there is a small transient observed before the steady state is reached. Droop controller apart from the synchronization between the parallel inverters also takes care of the power-sharing between the inverters. Both the real and reactive power of DER 1 and DER2 are shown in Figure 7 along with the direct and quadrature axis current at the load. Equal power sharing between both inverters is evident in the results thus obtained.

The results thus obtained at steady state operation of the DER 1 and DER2 are given in Figures 5-7. The load disturbance is applied on the islanded microgrids such that the out-of-synchronism condition occurs in the droop-controlled islanded microgrid due to the power capability limitations of renewable energy sources. Instability is introduced in the system by applying a load that is more than the capable power of the supply. The results obtained in case 2 are with the limitation of the PQ bus supplying 250 W of real power and 200 VAR. A high load of 2000 W is applied to introduce instability in the system. The results obtained after an increase in the load are given in Figures 8-10. The angular frequency of both the DERs has gone out of synchronism as shown in Figure 8. Direct and quadrature axis current and voltage waveform at the LCL filter is as given in Figure 9. Real power, reactive power, and direct and quadrature axis current of both DERs are given in Figure 10.

For both the steady-state and unstable simulations of the islanded microgrid, all 36 state space variables are monitored as specified in (25). Figure 11 depicts a correlation diagram of these state space variables, offering a visual representation of the interrelationships among various variables. Upon examination, it is observed that while some variables exhibit higher correlations, the majority of the variables do not display strong correlations. Therefore, all 36 variables are considered for the prediction algorithm, except for a few cases. This approach ensures that no important information is overlooked, as each variable may contribute to the overall prediction accuracy in a unique way. Thus, the inclusion of all variables enhances the robustness and reliability of the prediction algorithm, enabling it to effectively capture the complex relationships within the system. PCA multivariate variation graph for the 36 state space variables is given in Figure 12.

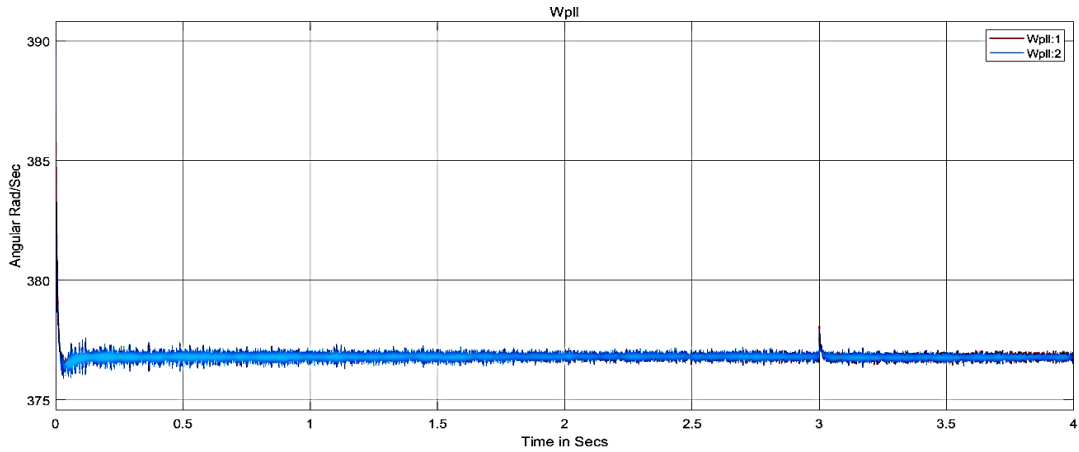


Figure 5. Angular rad/sec for both DER1 and DER2

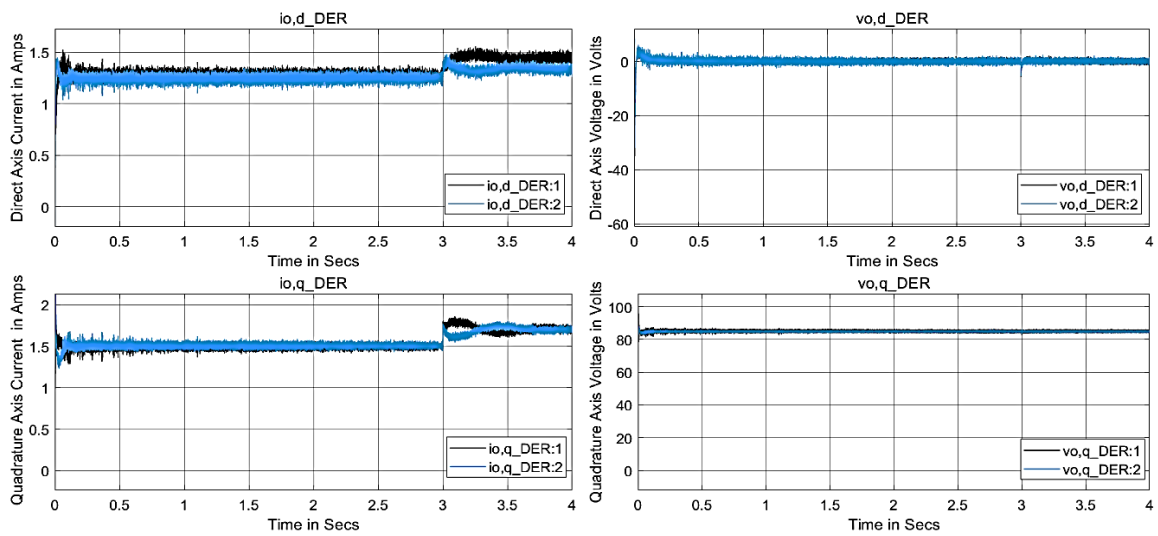


Figure 6. Direct axis and quadrature axis current and voltage at LCL filter

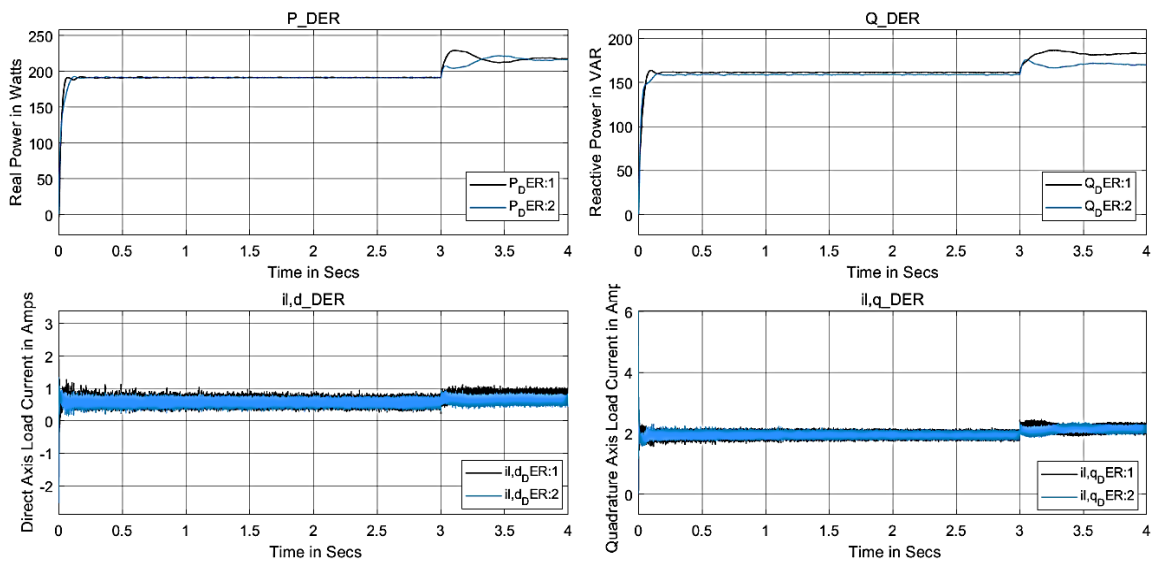


Figure 7. Real power, reactive power, direct axis current, quadrature current of DER1 and DER2

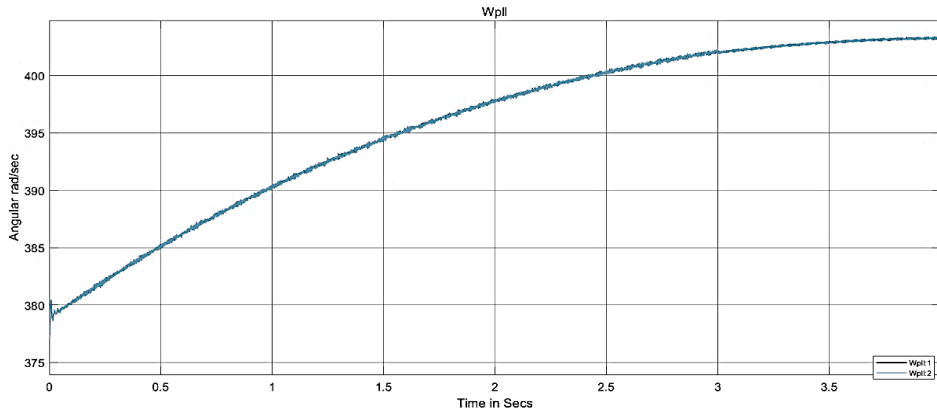


Figure 8. Angular rad/sec during instability

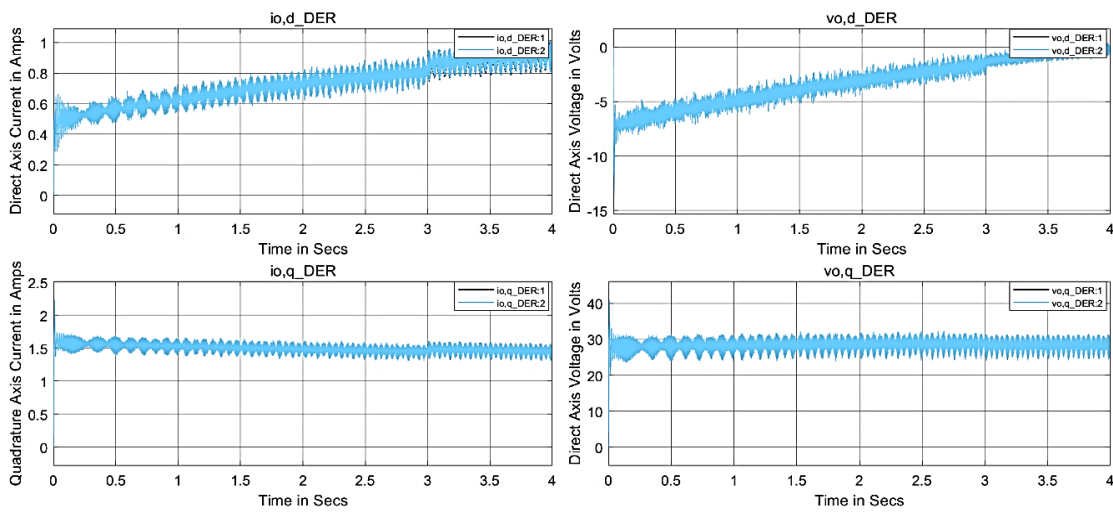


Figure 9. Direct axis and quadrature axis current and voltage at LCL filter

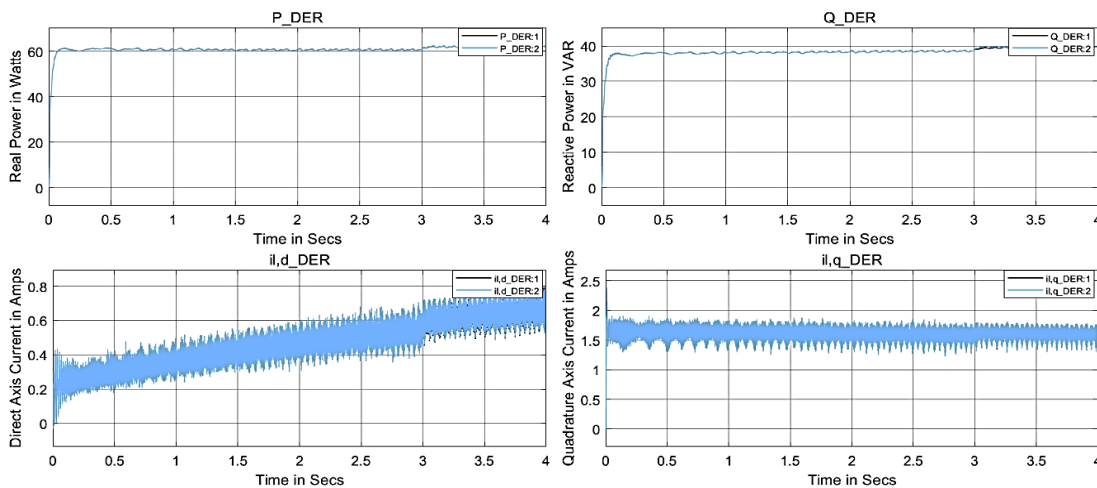


Figure 10. Real power, reactive power, direct axis current, quadrature current of DER1 and DER2

The SVM-based steady-state assessment is implemented using the PC1 since it represents 99 percent of the state space variables. The classification accuracy is observed to be 93.5% and the receiver operating characteristic (ROC) is obtained for the SVM implementation and the area under the curve (AUC) is obtained to be 0.95 as shown in Figure 13. The confusion matrix obtained for the SVM classification of steady state in

an islanded microgrid is given in Figure 14. With an accuracy of 93.5% and AUC of 0.95 in the ROC-AUC curve and good confusion matrix parameters, the SVM-based steady-state assessment is found to be satisfactory. Algorithms with better performance can be implemented to further improve the performance of the steady state assessment since it is dependent on the distribution system that supplies the customers.

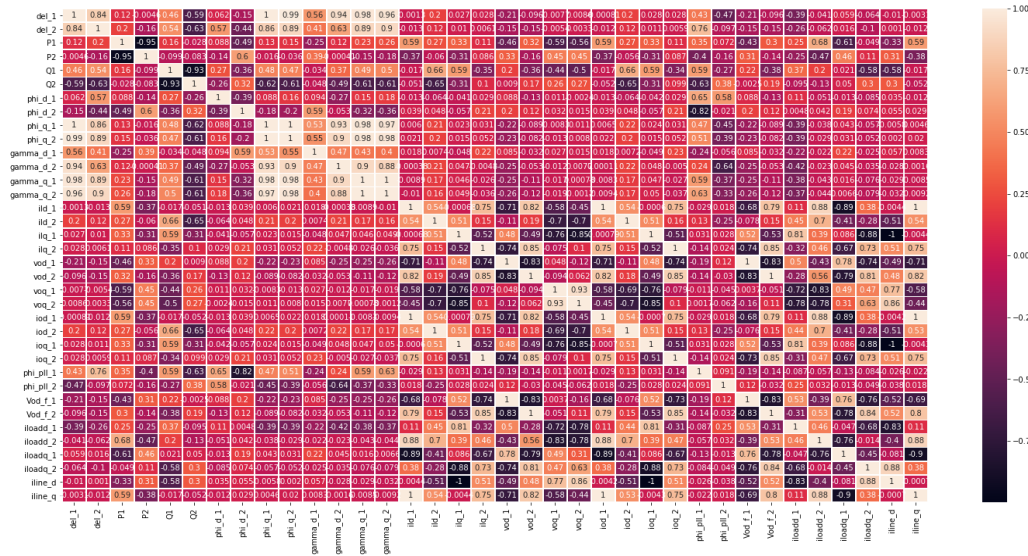


Figure 11. Correlation diagram of the state space variables

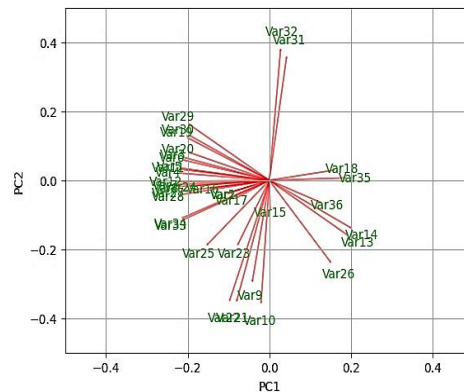


Figure 12. Principal component analysis plot showing multivariate variation for 36 variables

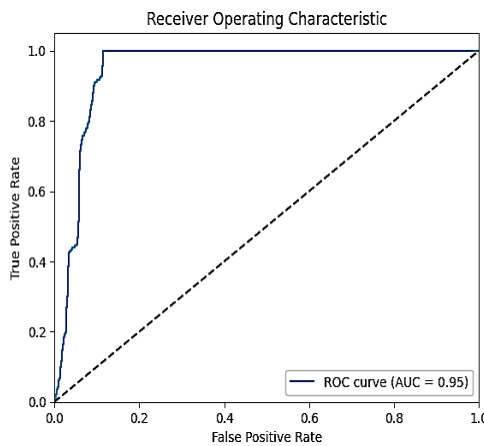


Figure 13. AUC-ROC curve

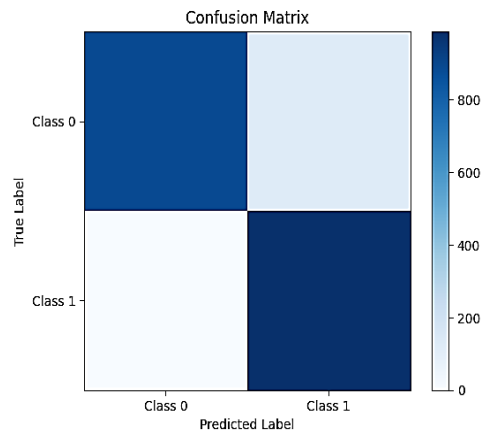


Figure 14. Confusion matrix

4. CONCLUSION

In conclusion, this study employs the support vector machine (SVM) algorithm to predict the steady-state stability of droop-controlled islanded microgrids. A comprehensive model of the islanded microgrid involving multiple inverters is constructed within the MATLAB Simulink platform. In order to streamline the variables, principal component analysis (PCA) is employed on the state space variables derived from the average model. This process entails extracting characteristics from the state space variables and consolidating them into the principal component (PC1), facilitating the development of an SVM classification algorithm. The steady-state assessment using SVM achieves an accuracy of 93.5%. Although the accuracy is reasonably high, there is still room for improvement by implementing more advanced algorithms to enhance performance further. Overall, this work shows the possibility of applying SVM and PCA methods for steady-state stability evaluation in droop-controlled islanded microgrids, with the results serving as a starting point for further investigation and improvements in microgrid stability analysis.

REFERENCES

- [1] B. Dağ and M. T. Aydemir, "A simplified stability analysis method for LV inverter-based microgrids," *Journal of Modern Power Systems and Clean Energy*, vol. 7, no. 3, pp. 612–620, May 2019, doi: 10.1007/s40565-018-0478-1.
- [2] S. Rajamand, "Synchronous generator control concept and modified droop for frequency and voltage stability of microgrid including inverter-based DGs," *Journal of Electrical Engineering and Technology*, vol. 15, no. 3, pp. 1035–1044, May 2020, doi: 10.1007/s42835-020-00383-z.
- [3] E. Sanabria, A. Chica, and S. Díaz, "Power-sharing controller of microgrid based on parallel inverters under the droop technique," in *Lecture Notes in Electrical Engineering*, vol. 685 LNEE, 2021, pp. 404–413.
- [4] K. Veerashekar, S. Eichner, and M. Luther, "Modelling and transient stability analysis of interconnected autonomous hybrid microgrids," in *2019 IEEE Milan PowerTech, PowerTech 2019*, Jun. 2019, pp. 1–6, doi: 10.1109/PTC.2019.8810589.
- [5] H. Alenius, M. Berg, R. Luhtala, T. Roinila, and T. Messo, "Impedance-based stability analysis of multi-parallel inverters applying total source admittance," in *2019 IEEE 20th Workshop on Control and Modeling for Power Electronics, COMPEL 2019*, Jun. 2019, pp. 1–8, doi: 10.1109/COMPEL.2019.8769695.
- [6] A. Rodríguez-Cabero and M. Prodanovic, "Stability analysis for weak grids with power electronics interfaces," in *IECON Proceedings (Industrial Electronics Conference)*, Oct. 2016, pp. 2402–2407, doi: 10.1109/IECON.2016.7793895.
- [7] R. E. Carballo and F. Botteron, "State space model for a droop control strategy with fault ride-through in UPS parallel inverters," in *Proceedings of the IEEE International Conference on Industrial Technology*, Mar. 2021, vol. 2021-March, pp. 494–501, doi: 10.1109/ICIT46573.2021.9453607.
- [8] W. Yang, H. Mi, M. Wang, and Z. Zeng, "Magnitude-resaping strategy of grid-connected inverter for improving stability of frequency coupling system in weak grids," in *2021 4th International Conference on Energy, Electrical and Power Engineering, CEEPE 2021*, Apr. 2021, pp. 564–569, doi: 10.1109/CEEPE51765.2021.9475741.
- [9] Y. Guo, L. Chen, X. Lu, J. Wang, T. Zheng, and S. Mei, "Region based stability analysis of active dampers in AC microgrids with multiple parallel interface inverters," in *Conference Proceedings - IEEE Applied Power Electronics Conference and Exposition - APEC*, Mar. 2019, vol. 2019-March, pp. 1098–1101, doi: 10.1109/APEC.2019.8721893.
- [10] M. Ahmed, L. Meegahapola, A. Vahidnia, and M. Datta, "Adaptive virtual impedance controller for parallel and radial microgrids with varying X/R ratios," *IEEE Transactions on Sustainable Energy*, vol. 13, no. 2, pp. 830–843, Apr. 2022, doi: 10.1109/TSTE.2021.3133413.
- [11] J. Guo, T. Chen, B. Chaudhuri, and S. Y. R. Hui, "Stability of isolated microgrids with renewable generation and smart loads," *IEEE Transactions on Sustainable Energy*, vol. 11, no. 4, pp. 2845–2854, Oct. 2020, doi: 10.1109/TSTE.2020.2980276.
- [12] H. R. Baghaee, M. Mirsalim, and G. B. Gharehpetian, "Performance improvement of multi-DER microgrid for small- and large-signal disturbances and nonlinear loads: Novel complementary control loop and fuzzy controller in a hierarchical droop-based control scheme," *IEEE Systems Journal*, vol. 12, no. 1, pp. 444–451, Mar. 2018, doi: 10.1109/JSYST.2016.2580617.
- [13] B. Wei, A. Marzabal, R. Ruiz, J. M. Guerrero, and J. C. Vasquez, "DAVIC: A new distributed adaptive virtual impedance control for parallel-connected voltage source inverters in modular UPS system," *IEEE Transactions on Power Electronics*, vol. 34, no. 6, pp. 5953–5968, Jun. 2019, doi: 10.1109/TPEL.2018.2869870.
- [14] B. Liu, Z. Liu, J. Liu, R. An, H. Zheng, and Y. Shi, "An adaptive virtual impedance control scheme based on small-AC-signal injection for unbalanced and harmonic power sharing in islanded microgrids," *IEEE Transactions on Power Electronics*, vol. 34, no. 12, pp. 12333–12355, Dec. 2019, doi: 10.1109/TPEL.2019.2905588.
- [15] M. Eskandari, L. Li, M. H. Moradi, F. Wang, and F. Blaabjerg, "A control system for stable operation of autonomous networked microgrids," *IEEE Transactions on Power Delivery*, vol. 35, no. 4, pp. 1633–1647, Aug. 2020, doi: 10.1109/TPWRD.2019.2948913.
- [16] M. Ahmed, L. Meegahapola, A. Vahidnia, and M. Datta, "Analyzing the effect of X/R ratio on dynamic performance of microgrids," in *Proceedings of 2019 IEEE PES Innovative Smart Grid Technologies Europe, ISGT-Europe 2019*, Sep. 2019, pp. 1–5, doi: 10.1109/ISGTEurope.2019.8905556.
- [17] L. Liang, Y. Hou, and D. J. Hill, "Enhancing flexibility of an islanded microgrid with electric springs," *IEEE Transactions on Smart Grid*, vol. 10, no. 1, pp. 899–909, Jan. 2019, doi: 10.1109/TSG.2017.2754545.
- [18] Y. Wang, X. Wang, Z. Chen, and F. Blaabjerg, "Small-signal stability analysis of inverter-fed power systems using component connection method," *IEEE Transactions on Smart Grid*, vol. 9, no. 5, pp. 5301–5310, Sep. 2018, doi: 10.1109/TSG.2017.2686841.
- [19] D. Chakravorty, J. Guo, B. Chaudhuri, and S. Y. R. Hui, "Small signal stability analysis of distribution networks with electric springs," *IEEE Transactions on Smart Grid*, vol. 10, no. 2, pp. 1543–1552, Mar. 2019, doi: 10.1109/TSG.2017.2772224.
- [20] B. Fan *et al.*, "A novel droop control strategy of reactive power sharing based on adaptive virtual impedance in microgrids," *IEEE Transactions on Industrial Electronics*, vol. 69, no. 11, pp. 11335–11347, Nov. 2022, doi: 10.1109/TIE.2021.3123660.
- [21] W. Zhang, Z. Zheng, and H. Liu, "Droop control method to achieve maximum power output of photovoltaic for parallel inverter system," *CSEE Journal of Power and Energy Systems*, vol. 8, no. 6, pp. 1636–1645, 2022, doi: 10.17775/CSEEJPES.2020.05070.
- [22] Y. Yang and R. J. Wai, "Self-constructing fuzzy-neural-network-imitating sliding-mode control for parallel-inverter system in grid-connected microgrid," *IEEE Access*, vol. 9, pp. 167389–167411, 2021, doi: 10.1109/ACCESS.2021.3135856.
- [23] T. Fang, S. Shen, Y. Jin, and X. Ruan, "Robustness investigation of multi-inverter paralleled grid-connected system with LCL-filter based on the grid-impedance allocation mechanism," *IEEE Transactions on Power Electronics*, vol. 36, no. 12, pp. 14508–14524, 2021, doi: 10.1109/TPEL.2021.3088992.

- [24] B. Liu, Z. Liu, and J. Liu, "A noninvasive feeder impedance estimation method for parallel inverters in microgrid based on load harmonic current," *IEEE Transactions on Power Electronics*, vol. 36, no. 7, pp. 7354–7359, 2021, doi: 10.1109/TPEL.2020.3042700.
- [25] Y. Qi, H. Deng, J. Wang, and Y. Tang, "Passivity-based synchronization stability analysis for power-electronic-interfaced distributed generations," *IEEE Transactions on Sustainable Energy*, vol. 12, no. 2, pp. 1141–1150, Apr. 2021, doi: 10.1109/TSTE.2020.3035261.
- [26] X. Peng and H. Yang, "Stability analysis of multi-paralleled grid-connected inverters including distribution parameter characteristics of transmission lines," *CSEE Journal of Power and Energy Systems*, vol. 7, no. 1, pp. 93–104, 2021, doi: 10.17775/CSEEJPES.2019.01530.
- [27] S. Zhou *et al.*, "An improved design of current controller for LCL-type grid-connected converter to reduce negative effect of PLL in weak grid," *IEEE Journal of Emerging and Selected Topics in Power Electronics*, vol. 6, no. 2, pp. 648–663, 2018, doi: 10.1109/JESTPE.2017.2780918.
- [28] M. Rasheduzzaman, J. A. Mueller, and J. W. Kimball, "An accurate small-signal model of inverter-dominated islanded microgrids using (dq) reference frame," *IEEE Journal of Emerging and Selected Topics in Power Electronics*, vol. 2, no. 4, pp. 1070–1080, Dec. 2014, doi: 10.1109/JESTPE.2014.2338131.
- [29] Y. Boujoudar *et al.*, "Fuzzy logic-based controller of the bidirectional direct current to direct current converter in microgrid," *International Journal of Electrical and Computer Engineering (IJECE)*, vol. 13, no. 5, p. 4789, Oct. 2023, doi: 10.11591/ijece.v13i5.pp4789-4797.
- [30] J. Kaur and A. Khosla, "Simulation and harmonic analysis of hybrid distributed energy generation based microgrid system using intelligent technique," *Indonesian Journal of Electrical Engineering and Computer Science*, vol. 30, no. 3, p. 1287, Jun. 2023, doi: 10.11591/ijeecs.v30.i3.pp1287-1296.
- [31] R. Salyam and V. Margaret, "Source-load-variable voltage regulated cascaded DC/DC converter for a DC microgrid system," *International Journal of Electrical and Computer Engineering (IJECE)*, vol. 13, no. 1, p. 107, Feb. 2023, doi: 10.11591/ijece.v13i1.pp107-115.
- [32] K. K. Rout, D. P. Mishra, S. Mishra, S. Patra, and S. R. Salkuti, "Perturb and observe maximum power point tracking approach for microgrid linked photovoltaic system," *Indonesian Journal of Electrical Engineering and Computer Science (IJECS)*, vol. 29, no. 2, pp. 635–643, Feb. 2023, doi: 10.11591/ijeecs.v29.i2.pp635-643.
- [33] S. Ramamurthi and P. Ramasamy, "High step-up DC-DC converter with switched capacitor-coupled inductor and voltage multiplier module," *International Journal of Power Electronics and Drive Systems (IJPEDS)*, vol. 13, no. 3, p. 1599, Sep. 2022, doi: 10.11591/ijpeds.v13.i3.pp1599-1604.
- [34] Z. Alhadrawi, M. N. Abdullah, and H. Mokhlis, "Review of microgrid protection strategies: current status and future prospects," *TELKOMNIKA (Telecommunication Computing Electronics and Control)*, vol. 20, no. 1, p. 173, Feb. 2022, doi: 10.12928/telkomnika.v20i1.19652.
- [35] D. Sattianadan, G. R. P. Kumar, R. Sridhar, K. V. Reddy, B. S. U. Reddy, and P. Mamatha, "Investigation of low voltage DC microgrid using sliding mode control," *International Journal of Power Electronics and Drive Systems (IJPEDS)*, vol. 11, no. 4, p. 2030, Dec. 2020, doi: 10.11591/ijpeds.v11.i4.pp2030-2037.
- [36] H. Afianti, O. Penangsang, and A. Soeprijanto, "Stability and reliability of low voltage hybrid AC-DC microgrids power flow model in islanding operation," *Indonesian Journal of Electrical Engineering and Computer Science (IJECS)*, vol. 19, no. 1, pp. 32–41, Jul. 2020, doi: 10.11591/ijeecs.v19.i1.pp32-41.

BIOGRAPHIES OF AUTHORS



Ganeshan Viswanathan    is a research scholar pursuing his research at Visvesvaraya Technological University (VTU) at the Department of Electronics and Communication Engineering, Dr. Ambedkar Institute of Technology, Bangalore, Karnataka, India. His subject of interest includes microgrid, power electronics, and embedded systems. He can be contacted at email: ganeshanvisu@gmail.com.



Govindanayakanapalya Venkatagiriappa Jayaramaiah    is currently working as a Professor and Head at the Electrical and Electronics Engineering Department, Dr. Ambedkar Institute of Technology, Bangalore. He has published many papers and written some books. His area of research is energy harvesting, power electronics, and embedded systems. He can be contacted at email: gvjayaram@gmail.com.